Applied Catalysis B: Environmental 324 (2023) 122236

Contents lists available at ScienceDirect

Applied Catalysis B: Environmental

journal homepage: www.elsevier.com/locate/apcatb

# Shifting reaction path for levulinic acid aqueous-phase hydrogenation by Pt-$TiO_2$ metal-support interaction

Fanchun Meng [a,b], Xinchun Yang [a,b], Shichao Zhao [a], Zhuo Li [a,b], Guikai Zhang [c], Yuntao Qi [a,b], Shengqi Chu [c], Guofu Wang [a], Jing Zhang [c], Yong Qin [a,b,*], Bin Zhang [a,b,*]

[a] State Key Laboratory of Coal Conversion, Institute of Coal Chemistry, Chinese Academy of Sciences, Taiyuan 030001, China
[b] Center of Materials Science and Optoelectronics Engineering, University of Chinese Academy of Sciences, Beijing 100049, China
[c] Beijing Synchrotron Radiation Facility, Institute of High Energy Physics, Chinese Academy of Sciences, Beijing 100049, China

ARTICLE INFO

*Keywords:*
Aqueous-phase
Levulinic acid hydrogenation
Pt-$TiO_2$ interaction
Reaction path shift
γ-valerolactone

ABSTRACT

Levulinic acid (LA) aqueous-phase hydrogenation into γ-valerolactone (GVL) is considered one of the pivotal reactions to convert biomass into renewable chemicals. Here we have deposited Pt on $TiO_2$ nanofilm coated α-$Al_2O_3$ via atomic layer deposition (ALD) to synthesize Pt-$TiO_2$/α-$Al_2O_3$. This catalyst shows excellent activity and stability (1000 h) in LA hydrogenation compared to Pt/α-$Al_2O_3$. By excluding the effect of Pt particle size, lattice plane, support morphology, pore structure, and electronic state, the critical role of Pt-$TiO_2$ interaction is revealed by various characterization methods. CO diffuse reflectance infrared Fourier transform spectroscopy (DRIFTS) and in-situ Fourier transform Infrared spectra (FTIR) results indicate that Pt-$TiO_2$ interaction provides new interfacial Pt sites for LA and intermediate adsorption and Ti-OH active sites for LA dehydration cyclization to α-angelica lactone intermediate, which leads to the shift of reaction pathways from direct LA C═O hydrogenation lactonization on Pt/α-$Al_2O_3$ to LA dehydration cyclization and hydrogenation on Pt-$TiO_2$/α-$Al_2O_3$. It provides insight into the design of high-efficient catalysts for aqueous-phase hydrogenation.

## 1. Introduction

Supported metal catalysts have been developed for the aqueous-phase hydrogenation of biomass-derived oxygenates to fuels and fine chemicals [1–6]. For example, Levulinic acid (LA) aqueous-phase hydrogenation into γ-valerolactone (GVL) is considered one of the pivotal reactions to convert lignocellulose-based biomass into renewable fuels and chemicals [7–10]. Although the Pt-based catalysts perform high efficiency in hydrogenation, their catalytic activity is lower than Ru-based catalysts in aqueous-phase LA hydrogenation. In general, Pt-based catalysts face the same challenges as Ru-based catalysts in aqueous-phase LA hydrogenation, such as corrosion of acidic solvent at high temperatures, mass transport limitations, competitive adsorption, and unexpected structural transformations of catalyst [11]. Furthermore, the role of water is always ignored for Pt-catalyzed hydrogenation of LA or acetone since the initial activities are not sensitive to water solvent [12]. However, we need to notice that the stability of Pt-based catalysts is low during LA aqueous phase hydrogenation [13]. Therefore, developing a highly efficient Pt-based catalyst in LA aqueous-phase hydrogenation is still highly desirable.

Recent results show that the metal-support interaction (MSI) alters the geometric morphologies, electronic properties, or distribution of metal nanoparticles, influencing the catalytic activity of supported metal catalysts [14–16]. In order to increase the activity and stability of metal catalysts in water, the tailoring of metal-support interaction will be an effective strategy. $TiO_2$ is a promising water-tolerant solid acid support of metal nanoparticles [17]. Strong Pt-$TiO_2$ interaction and Pt-O-Ti bonding induce a high sinter resistivity at high temperatures for many reactions [18]. Despite the significant progress and valuable insights from previous investigations, the specific effects of water have not been systematically revealed to date, and the complex functions of the Pt-$TiO_2$ interaction in the aqueous-phase hydrogenation of LA remain elusive.

In this work, we have deposited Pt nanoparticles on $TiO_2$ nanofilm modified α-$Al_2O_3$ and α-$Al_2O_3$ to synthesize Pt-$TiO_2$/α-$Al_2O_3$ and Pt/α-$Al_2O_3$ by atomic layer deposition (ALD). Because of the self-limited property of ALD, these two catalysts have identical Pt particle size, support morphology, and pore structure for straightforwardly exploring

* Corresponding authors at: State Key Laboratory of Coal Conversion, Institute of Coal Chemistry, Chinese Academy of Sciences, Taiyuan 030001, China
*E-mail addresses:* qinyong@sxicc.ac.cn (Y. Qin), zhangbin2009@sxicc.ac.cn (B. Zhang).

https://doi.org/10.1016/j.apcatb.2022.122236
Received 5 September 2022; Received in revised form 25 November 2022; Accepted 27 November 2022
Available online 29 November 2022

the functions of the Pt-$TiO_2$ interaction on catalytic performance. Compared to Pt/α-$Al_2O_3$ and reported Pt-based catalysts, Pt-$TiO_2$/α-$Al_2O_3$ shows higher activity and stability in aqueous-phase LA hydrogenation to GVL after building Pt-$TiO_2$ interaction. Based on various characterizations, it is found that Pt-$TiO_2$ interaction facilities the adsorption of LA and water. The Ti-OH sites for the direct LA cyclization and water adsorption after the formation of Pt-$TiO_2$ interaction lead to the reaction pathway shifts from C═O bond hydrogenation and cyclization to cyclization and C═C bond hydrogenation.

## 2. Experimental

### 2.1. Synthesis of catalysts

The ALD process was carried out in a homemade closed-chamber type ALD reactor. High-purity $N_2$ (99.999%) was utilized as a carrier gas. The Pt ALD was carried out by alternately dosing Trimethyl (methylcyclopentadienyl)platinum(IV) ($MeCpPtMe_3$) and $O_3$ at 150 °C. $MeCpPtMe_3$ was kept at 75 °C. The pulse, exposure, and purge time for the $MeCpPtMe_3$ precursor were 0.5, 15, and 30 s, and those for $O_3$ were 0.5, 10, and 30 s, respectively. The ALD $TiO_2$ film was grown by sequentially exposing α-$Al_2O_3$ to titanium tetraisopropoxide and ultrapure water at 150 °C. Titanium tetraisopropoxide and water were kept at 80 °C and 25 °C, respectively. The pulse, exposure, and purge times for titanium tetraisopropoxide were 1, 8, and 20 s, and those for $H_2O$ were 0.1, 8, and 25 s, respectively. Pt/α-$Al_2O_3$ was synthesized by depositing 20 cycles of Pt on α-$Al_2O_3$. And 20 cycles of Pt were also deposited on different supports to prepare Pt/γ-$Al_2O_3$, Pt/$CeO_2$, Pt/$ZrO_2$, and Pt/P25. In order to modify the surface of α-$Al_2O_3$ without changing its texture, 40 cycles of $TiO_2$ were deposited on α-$Al_2O_3$ to obtain a layer of 3.5 nm thickness. Then, 20 cycles of Pt were deposited on $TiO_2$/α-$Al_2O_3$ for the preparation of Pt-$TiO_2$/α-$Al_2O_3$. To explore the universality of building Pt-$TiO_2$ interaction for high-efficiency hydrogenation in the aqueous phase, we have sequentially deposited the $TiO_2$ layer of 40 cycles and Pt nanoparticles of 20 cycles on different common supports for preparing Pt-$TiO_2$/γ-$Al_2O_3$, Pt-$TiO_2$/$CeO_2$, Pt-$TiO_2$/$ZrO_2$, and Pt-$TiO_2$/P25, respectively.

### 2.2. Catalyst characterization

The transmission electron microscopy (TEM), high-resolution transmission electron microscope (HRTEM), and scanning transmission electron microscopy (STEM) images were acquired on a JEOL-2100 F microscope. The X-ray diffraction (XRD) was carried out on a RIGAKU MiniFlex II desktop X-ray diffractometer operating with Cu Kα source (λ = 1.540 Å) at 40 kV and 40 mA at a scanning speed (2θ) of 5°/min and a scanning range of 10°—90°. The contents of Pt and Ti were determined based on inductively coupled plasma mass spectrometry (ICP-MS Agilent 7900) analysis. The X-ray photoelectron spectra (XPS) were recorded on an ES-300 photoelectron spectrometer (KRATOS Analytical). The XPS spectra of the catalysts were recorded after the LA hydrogenation for 0.5 h. The X-ray absorption fine spectra (XAFS) results were obtained on the 1W1B beamline equipped with a fixed-exit Si (111) double-crystal monochromator in Beijing Synchrotron Radiation Facility (BSRF), Institute of High Energy Physics, Chinese Academy of Sciences. Pt foil was used as a reference sample. The Pt $L_3$-edge X-ray absorption near-edge structure (XANES) and extended X-ray absorption fine structure (EXAFS) spectra for the catalysts were measured in fluorescence mode. The XANES and Fourier transform EXAFS data from the X-ray absorption spectra (XAS) analysis were fitted with the ATHENA and ARTEMIS software programs. CO pulse chemisorption was carried out on Micromeritics AutoChem II volumetric adsorption analyzer. Diffuse reflectance infrared Fourier transform spectroscopy (DRIFTS) spectra were recorded on Bruker Tensor II IR spectrometer with a resolution of 4 $cm^{-1}$. The samples were placed inside a synchrotron cell with a ZnSe window. Before CO adsorption at 30 °C, the sample was reduced in 10% $H_2$/Ar at 200 °C for 1 h. We have also revealed the sites for LA and intermediate adsorption by CO-DRIFTS on the catalyst after LA adsorption and hydrogenation at 150 °C.

### 2.3. Catalytic performance evaluation

Aqueous-phase catalytic hydrogenation of LA to GVL was performed in a 50 mL autoclave at various temperatures (120–150 °C) and a (cold) $H_2$ pressure of 3.0 MPa. In a typical reaction, 8.6 mmol LA and 10 mg catalyst were loaded into the autoclave. A 5.0 mL degassed water was injected into the autoclave. The autoclave was then sealed and purged four times with $H_2$ before the pressure was increased to 3.0 MPa. The reaction was started by heating the autoclave to the desired reaction temperature under continuous stirring (700 rpm). After the reaction, the autoclave was cooled rapidly to room temperature in an ice bath, after which the remaining $H_2$ was released. The catalyst was separated from the solution by filtration. The stability evaluation of Pt-$TiO_2$/α-$Al_2O_3$ was carried out in a tubular fixed-bed microreactor. Prior to the reaction, the 50 mg catalyst was reduced in pure $H_2$ at 300 °C for 2 h. After the reactor's temperature and pressure reached reaction conditions, a 10 wt% (by weight) aqueous solution of LA was pumped into a vaporizer, mixed with a carrier gas (40 mL/min $H_2$), and then introduced into the reactor. The total pressure in the reactor was kept at 3.0 MPa. The reaction products were analyzed by GC (GC-9720, Zhejiang Fuli chromatogram analysis Co., Ltd., China) equipped with a hydrogen flame ionization detector (FID) and a capillary column (HP-5, 30 m × 0.32 mm). And 1,4-dioxane was used as an internal standard.

The conversion of LA ($X_{LA}$) was calculated as follows:

$$X_{LA} = \frac{M_{0,LA} - M_{t,LA}}{M_{0,LA}} \times 100\%$$

The yield of the liquid component ($Y_{GVL}$) was calculated as follows:

$$Y_{GVL} = \frac{M_{t,GVL}}{M_{theoretical,GVL}} \times 100\%$$

$M_{0,\,LA}$ corresponds to the initial LA mass fraction. $M_{t,\,LA}$ and $M_{t,GVL}$ represent the mass fraction of LA and GVL in the withdrawn sample at reaction time (t). Finally, $M_{theoretical,GVL}$ is the calculated mass fraction assuming a complete conversion of LA to GVL. Stability tests were applied in a fixed-bed reactor. Additionally, the turnover frequency (TOF) was calculated as:

$$TOF = \frac{n_{LA}}{n_{Pt} \times D_{Pt}},$$

Where $n_{LA}$ is the molar amount of LA converted after 1 h of reaction time, $n_{Pt}$ is the molar Pt amount in the catalyst, and $D_{Pt}$ is Pt dispersion determined by CO-chemisorption.

## 3. Results and discussion

### 3.1. The structure of Pt-based catalyst after building Pt-$TiO_2$ interaction

α-$Al_2O_3$ nanoparticles were utilized as the water-tolerated inert support. $TiO_2$ layer (40 cycles, ~3.5 nm, Fig. S1) coated α-$Al_2O_3$ (denoted as $TiO_2$/α-$Al_2O_3$) was also prepared for comparison. Then, 20 cycles of Pt were deposited on the α-$Al_2O_3$ and $TiO_2$/α-$Al_2O_3$ to obtain Pt/α-$Al_2O_3$ and Pt-$TiO_2$/α-$Al_2O_3$, respectively (Scheme 1). HRTEM images ( Fig. 1a-d, Fig. S2) show that these two catalysts perform the same Pt particle size (~2.4 nm) and visible adjacent lattice fringes (0.225 nm, Pt(111)). The high-angle annular dark-field scanning transmission electron microscopy (HAADF-STEM) (Figs. 1e and 1f) and energy dispersive X-ray (EDX) spectrometry images (Figs. 1g and 1h, Fig. S3) further indicate that the amorphous $TiO_2$ layer was deposited on α-$Al_2O_3$, and Pt, Ti elements were homogeneously dispersed on the surface of α-$Al_2O_3$. Therefore, the $TiO_2$ layer does not change the Pt nanoparticles' size and crystal structure. Because of the ultrathin thickness of the $TiO_2$ layer, the surface area and crystal structure of Pt

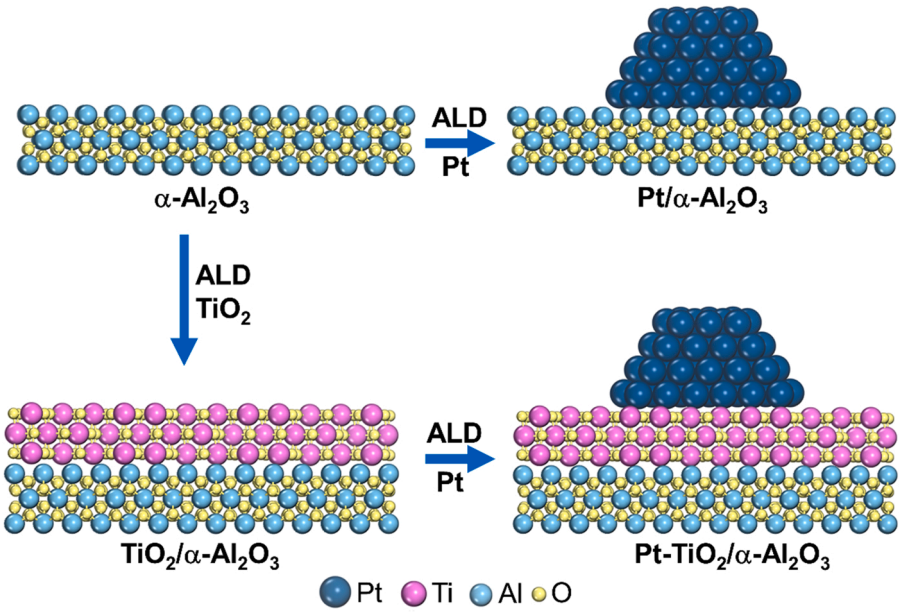


**Scheme 1.** Schematic illustration of the synthesis process of Pt/α-$Al_2O_3$ and Pt-$TiO_2$/α-$Al_2O_3$.

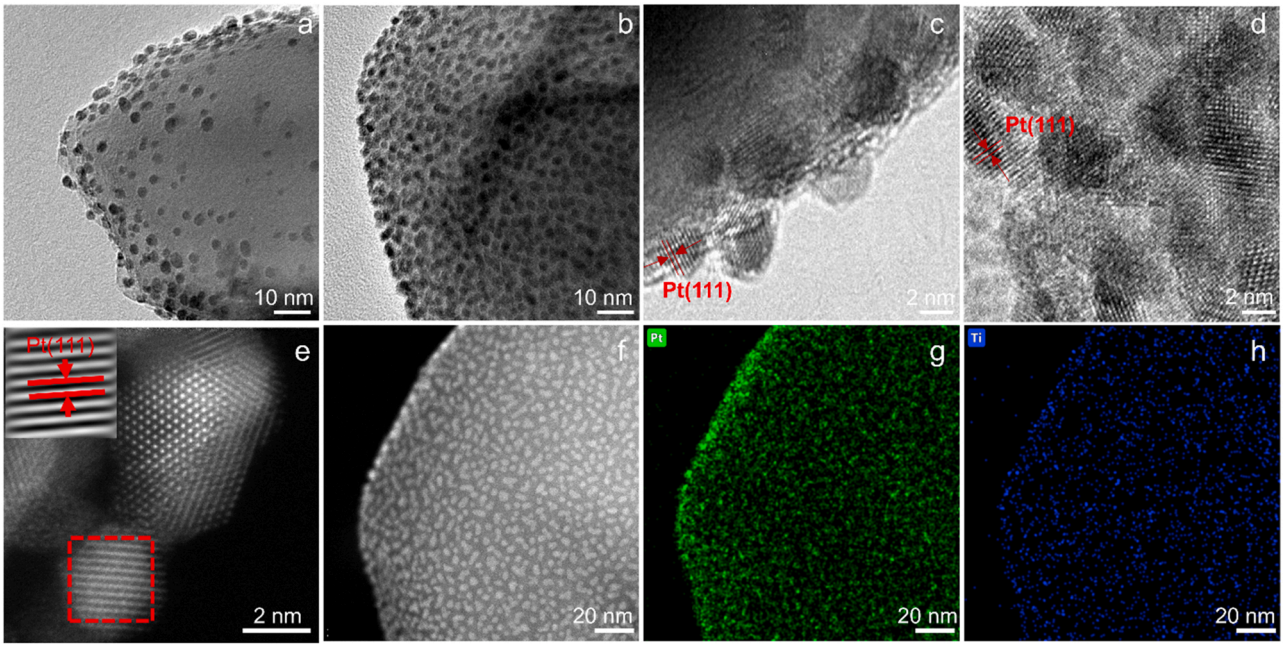


**Fig. 1.** Morphology of Pt/α-$Al_2O_3$ and Pt-$TiO_2$/α-$Al_2O_3$. TEM and HRTEM images of Pt/α-$Al_2O_3$ (a, c) and Pt-$TiO_2$/α-$Al_2O_3$ (b, d). (e, f) Cs-corrected HAADF-STEM images of Pt-$TiO_2$/α-$Al_2O_3$. (g, h) EDX element mapping of Pt and Ti on Pt-$TiO_2$/α-$Al_2O_3$.

will be maintained after the formation of Pt-$TiO_2$ interaction. Fig. S4 and Table S1 show that the two catalysts perform the same $N_2$ adsorption-desorption isotherms (ADI, type II), with similar surface area and pore distribution. Fig. S5 shows the XRD patterns of Pt/α-$Al_2O_3$ and Pt-$TiO_2$/α-$Al_2O_3$. All the samples exhibit the characteristic peaks of α-$Al_2O_3$. In addition, no evident Pt and $TiO_2$ reflections are detected, indicating the high dispersion of Pt and $TiO_2$. Considering particle size, lattice plane, pore structure, and morphology of the Pt/α-$Al_2O_3$ and Pt-$TiO_2$/α-$Al_2O_3$, we can investigate the function of the Pt-$TiO_2$ interaction in LA hydrogenation.

Figs. 2a and b display the Pt 4d and Ti-2p XPS spectra after the reaction to reveal the metal's electric state. The Pt $4d_{5/2}$ were fitted into three peaks at 314.5 eV, 316.9 eV, and 318.5 eV, attributed to $Pt^0$, $Pt^{2+}$, and $Pt^{4+}$ species, respectively [19,20]. The binding energy and ratio of $Pt^0$ (majority of species) are nearly the same over Pt/α-$Al_2O_3$ and Pt-$TiO_2$/α-$Al_2O_3$, indicating the Pt-$TiO_2$ interaction has a weak influence on the Pt electric state. Similar Ti 2p spectra of $TiO_2$/α-$Al_2O_3$ and Pt-$TiO_2$/α-$Al_2O_3$ verify that the electric state is not changed after the formation of Pt-$TiO_2$ interaction. Since $TiO_2$/α-$Al_2O_3$ and Pt-$TiO_2$/α-$Al_2O_3$ have similar Ti loading (Table S1), the lower intensity of XPS for Pt-$TiO_2$/α-$Al_2O_3$ is due to the deposition of Pt on $TiO_2$. XAFS illustrates Pt nanoparticles' electronic and coordinate structure. The "white line" intensities of Pt $L_3$-edge normalized XANES spectra for the two catalysts are similar to that of Pt foil, indicating that $Pt^0$ is the dominant species (Fig. 2c) [21,22]. The Fourier transforms (R space, Fig. 2d and Table S2) of EXAFS data of the two catalysts are also similar, indicating that the

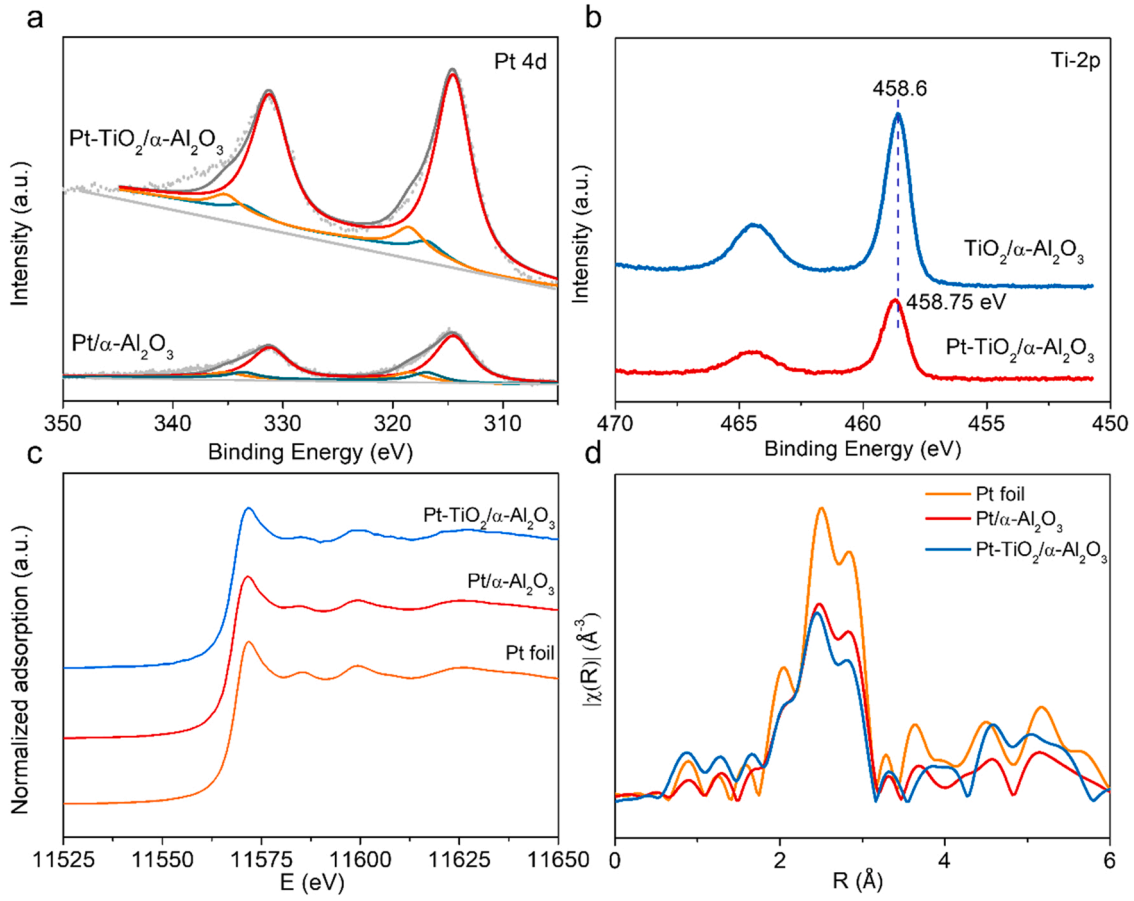


**Fig. 2.** Electronic structure. (a) Pt 4d XPS spectra of Pt/α-$Al_2O_3$ and Pt-$TiO_2$/α-$Al_2O_3$. (b) Ti 2p XPS spectra of $TiO_2$/α-$Al_2O_3$ and Pt-$TiO_2$/α-$Al_2O_3$. (c) The normalized intensity of XANES spectra of Pt-$L_3$. (d) The normalized intensity of Fourier transform weighted EXAFS spectra of Pt-$L_3$.

coordination and valence states of Pt nanoparticles did not change after forming the Pt-$TiO_2$ interaction.

### 3.2. Catalytic performance for LA hydrogenation

Fig. 3a shows the catalytic activity of Pt/α-$Al_2O_3$ and Pt-$TiO_2$/α-$Al_2O_3$ in aqueous-phase LA hydrogenation. Compared to Pt/α-$Al_2O_3$, higher catalytic activity was detected over Pt-$TiO_2$/α-$Al_2O_3$. The conversion of LA on Pt-$TiO_2$/α-$Al_2O_3$ reaches 36.9%, while the conversion of LA on Pt/α-$Al_2O_3$ is only 8.0% for 1 h reaction under identical conditions. Pt-$TiO_2$/α-$Al_2O_3$ is shown to be highly active in the hydrogenation of LA to GVL, with a LA conversion of 98.0% and a GVL selectivity of 98.3% in 3 h (Fig. 3b). The turnover frequency (TOF) is calculated from the CO-chemisorption and catalytic results at low conversion (<15%). At a temperature of 150 °C, the TOF over Pt-$TiO_2$/α-$Al_2O_3$ is 4943 $h^{-1}$ and ~2 times that over Pt/α-$Al_2O_3$ (2487 $h^{-1}$). The kinetic analysis further showed much lower apparent activation energy over Pt-$TiO_2$/α-$Al_2O_3$ (69.0 kJ/mol) than that over Pt/α-$Al_2O_3$ (79.8 kJ/mol) (Fig. 3c). Therefore, Pt-$TiO_2$ interaction favors the aqueous-phase LA hydrogenation.

The comparison between Pt-$TiO_2$/α-$Al_2O_3$ and the previously reported Pt and Ru-based catalysts is shown in Table S3. The TOF on Pt-$TiO_2$/α-$Al_2O_3$ is much higher than reported Pt-based catalysts and even close to those of the Ru-based catalysts [23]. Pt-$TiO_2$/α-$Al_2O_3$ also performed high stability and exhibited nearly similar activity after five consecutive recycling runs (Fig. S6). ICP-MS was utilized to test the Pt, Ti, and Al contents in the reaction solvent after the reaction at 150 °C. However, there was nearly no leaching of Pt, Ti, and Al into the solvent. We have also investigated the stability of Pt-$TiO_2$/α-$Al_2O_3$ in the aqueous-phase hydrogenation of LA in a fixed-bed reactor. Fig. 3d shows that Pt-$TiO_2$/α-$Al_2O_3$ is stable for 500 h at 150 °C. When further raised the reaction temperature to 190 °C, it remains stable for about 500 h with a GVL yield of 99%. Thus, Pt-$TiO_2$/α-$Al_2O_3$ shows both excellent catalytic activity and stability in acidic hydrothermal conditions.

### 3.3. The surface site for LA adsorption and hydrogenation

The CO diffuse reflectance Fourier transform infrared spectroscopy (CO-DRIFTS) was used to distinguish the different surface Pt active sites (Fig. 4a). The peaks between 2000 and 2100 $cm^{-1}$ and weak broad peaks below 2000 $cm^{-1}$ are characteristic of linearly and bridged adsorbed CO, respectively [24–26]. The main difference between Pt/α-$Al_2O_3$ and Pt-$TiO_2$/α-$Al_2O_3$ is the linearly adsorbed CO peaks between 2000 and 2100 $cm^{-1}$. We have fitted the linearly adsorbed CO on Pt-$TiO_2$/α-$Al_2O_3$ into three peaks at the position of 2087 $cm^{-1}$, 2063 $cm^{-1}$, and 2044 $cm^{-1}$, denoted as α, β, and γ sites of linely adsorbed CO on Pt nanoparticles. In contrast, only the β and γ sites are observed on Pt/α-$Al_2O_3$. Since Pt/α-$Al_2O_3$ and Pt-$TiO_2$/α-$Al_2O_3$ perform the same particle size and lattice structure of Pt nanoparticles, we can deduce that α sites originated from the Pt-$TiO_2$ interaction [27]. Considering the high wavenumber of CO at α sites, the Pt species are well-coordinated Pt atoms nearby $TiO_2$ with low electric density.[28,29] Accordingly, β sites centered at 2063 $cm^{-1}$ were assigned to higher coordination Pt sites [30], while γ sites at 2044 $cm^{-1}$ correspond to CO molecules that are linearly adsorbed on low-coordination Pt-edge and -corner sites. To explore the function of the above sites for LA adsorption, we carried out CO-DRIFTS after in-situ LA surface absorption (Fig. 4b, c). After the saturated adsorption of LA on the surface of Pt/α-$Al_2O_3$, the CO adsorption peak for β sites decreases, while the peak for γ sites is left. Thus, LA occupied part of the β sites, and γ sites cannot

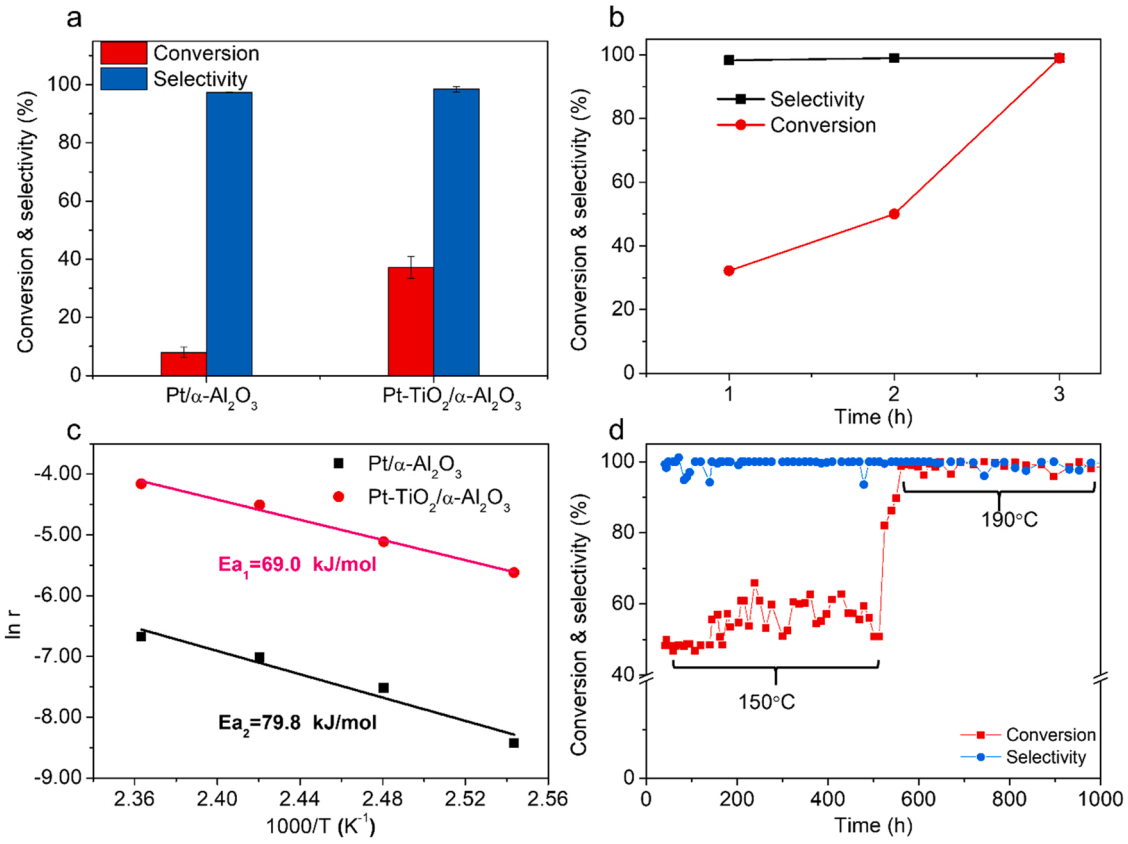


**Fig. 3.** Catalytic performance. (a) catalytic performance of Pt/α-$Al_2O_3$ and Pt-$TiO_2$/α-$Al_2O_3$ in an autoclave (reaction conditions:10 mg catalyst, 3 MPa, 8.6 mmol LA, 150 °C, 5 mL $H_2O$, 700 rpm, 1 h). (b) LA conversion as a function of reaction time over Pt-$TiO_2$/α-$Al_2O_3$ at 150 °C. (c) Kinetic activation energy calculations based on refined reaction rate (conversion < 15%). (d) Stability of Pt-$TiO_2$/α-$Al_2O_3$ for LA hydrogenation in a fixed bed reactor (reaction conditions: 50 mg catalyst, 3 MPa, 10% LA aqueous solution, 150 °C, and 190°C, 40 mL/min $H_2$).

adsorb LA on Pt/α-$Al_2O_3$. In addition to the occupation of β sites, α sites on Pt-$TiO_2$/α-$Al_2O_3$ disappear after LA adsorption. Therefore, Pt species from the Pt-$TiO_2$ interaction can strongly adsorb LA, leading to the enrichment of LA on the surface. LA enrichment is also revealed in XPS results, in which COOH species were detected over Pt-$TiO_2$/α-$Al_2O_3$ [31] (Fig. 4d).

We have conducted the CO-DRIFTS after saturated adsorption of LA and further reaction in $H_2$ at 150 °C at atmospheric pressure to reveal the reactivity of LA on different sites. For Pt/α-$Al_2O_3$, the β sites are consumed due to the adsorption of LA and intermediates, while the number of γ sites is not changed. For Pt-$TiO_2$/α-$Al_2O_3$, all the β sites disappear, and the intensity of γ sites decreases. Therefore, the LA adsorbed α sites are too strong for further hydrogenation. More stable intermediates are generated on surface β sites of Pt nanoparticles due to the Pt-$TiO_2$ interaction. In addition, all the γ sites cannot adsorb the LA and its intermediates. Because the electric density of different surface Pt sites increases with the order: α sites < β sites < γ sites, the Pt electric deficient α sites at the interface facilitate strong LA adsorption, and β sites with moderate electron density provide active sites for the adsorption of intermediates.

### 3.4. Reaction path and mechanism

We have investigated the reaction mechanism of LA hydrogenation through isotopic experiments. Since $D_2$ has nearly no isotope effect on LA hydrogenation to GVL ($kH_2/kD_2 \approx 1$, Fig. 5a), the activation of hydrogen is not the rate-limiting step for aqueous-phase hydrogenation of LA. The products were analyzed using GC-MS (Figs. S7a-c and 5d). However, the D atom was not observed in GVL when $D_2$ was the reductant. That is to say, the H in the product GVL is from the $H_2O$ solvent. Then, the LA hydrogenation on Pt/α-$Al_2O_3$ and Pt-$TiO_2$/α-$Al_2O_3$ was performed in $D_2O$. Interestingly, the catalytic activity on both catalysts was enhanced in $D_2O$. Significant $H_2O/D_2O$ inverse kinetic isotope effect [32,33] of 0.78 on Pt/α-$Al_2O_3$ (Fig. 5b) and 0.52 on Pt-$TiO_2$/α-$Al_2O_3$ (Fig. 5c) were detected. Therefore, water is indirectly involved in the rate-limiting step and plays a more significant role after forming Pt-$TiO_2$ interaction.

The products in the $D_2O$ solvent were carefully analyzed for Pt/α-$Al_2O_3$ (Fig. 5e) and Pt-$TiO_2$/α-$Al_2O_3$ (Fig. 5f). For GVL with no D, its *m/z* is 100. [1D]-GVL with an *m/z* of 101 (Scheme 2, Route 1) is the main product over Pt/α-$Al_2O_3$, while [2D]-GVL with an *m/z* of 102 (Scheme 2, Route 2) is the main product over Pt-$TiO_2$/α-$Al_2O_3$. This result indicates that the reaction route for aqueous-phase LA hydrogenation is changed after the formation of Pt-$TiO_2$ interaction. In general, the hydrogenation of LA happens through two routes (Scheme 2). For route 1, the D atom of water participated in the C═O group of LA hydrogenation, and [1D]-GVL will be generated after further lactonization in $D_2O$. This reaction route is mainly observed and discussed on Ru catalysts, even in the aqueous phase [9]. For route 2, LA is cyclized on acidic sites to produce the intermediate α-angelica lactone, which reacts with two D atoms to generate [2D]-GVL in $D_2O$. Considering the dominant production of [2D]-GVL on Pt-$TiO_2$/α-$Al_2O_3$, the Pt-$TiO_2$ interaction shifts the reaction route of LA hydrogenation from route 1 to route 2. Furthermore, the inverse solvent isotope effect can be correlated with the weaker H-bond with $D_2O$ compared to $H_2O$ [34], which will increase the acidity of the solvent for LA dehydration.

In-situ FTIR measurements were performed to obtain insights into the reaction mechanism. Fig. 6a shows in-situ FTIR difference spectra of the adsorption LA on Pt/α-$Al_2O_3$ and Pt-$TiO_2$/α-$Al_2O_3$ and $TiO_2$/α-$Al_2O_3$ in Ar flow at 150 °C. Characteristic peaks of LA are located at 1716 $cm^{-1}$

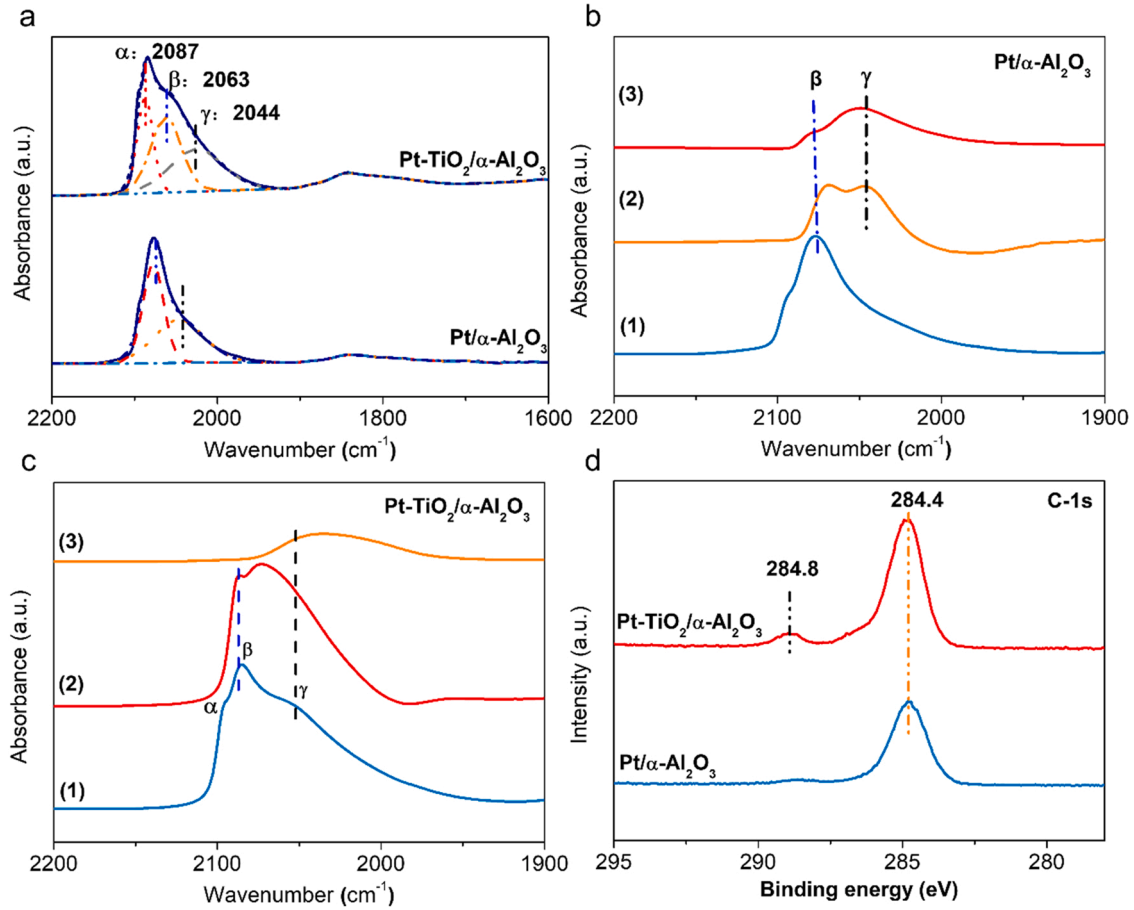


**Fig. 4.** Surface Pt sites for LA adsorption and hydrogenation. (a) Pt/α-$Al_2O_3$ and Pt-$TiO_2$/α-$Al_2O_3$. (b, c) CO DRIFTS spectra of Pt/α-$Al_2O_3$ and Pt-$TiO_2$/α-$Al_2O_3$ after adsorption of LA: (1) reduced catalyst, (2) reduced catalyst after LA saturated adsorption, (3) reduced catalyst after sequential LA saturated adsorption and $H_2$ treatment at 150 °C. (d) C 1 s XPS spectra of used Pt/α-$Al_2O_3$ and Pt-$TiO_2$/α-$Al_2O_3$.

(the C═O stretching modes [35]), 1450–1400 $cm^{-1}$, and 1600–1545 $cm^{-1}$ (the symmetric and asymmetric stretching frequencies of the carboxylate, $\nu_{sy}$ and $\nu_{asy}$ of COO [36]). The peak at 1783 $cm^{-1}$ is the C═O stretching for lactone. Only peaks of LA were detected when injecting LA aqueous solution on α-$Al_2O_3$ and Pt/α-$Al_2O_3$. However, a new peak appears at 1783 $cm^{-1}$, C═O stretching of intermediate α-angelica lactone from LA cyclization over $TiO_2$/α-$Al_2O_3$ and Pt-$TiO_2$/α-$Al_2O_3$. The results were in agreement with the isotope experiment, suggesting the reaction pathway shifts.

We carried out controlled experiments of water and LA adsorptions to reveal the role of water in reaction pathway shifts. Only the peaks of LA were observed when introducing pure LA on $TiO_2$/α-$Al_2O_3$ (Fig. 6a). The peak at 1783 $cm^{-1}$ for lactone is generated after injecting water, together with the formation new absorption band at 3516 $cm^{-1}$ for isolated hydroxyl groups on $TiO_2$ (Ti-OH) [37]. These Ti-OH species provide acidic sites for direct LA cyclization [38]. Stronger Ti-OH and adsorptive lactone peaks on Pt-$TiO_2$/α-$Al_2O_3$ further suggest that the Pt-$TiO_2$ interaction enhances water adsorption and Ti-OH formation [39].

To further confirm that lactone is intermediate, we carried out in situ surface reaction. When introducing 10% $H_2$/Ar on the surface of the samples with absorbed LA on α-$Al_2O_3$ and $TiO_2$/α-$Al_2O_3$, the IR spectrum is not changed, indicating that the two samples are inactive (Fig. S8a and b). On the contrary, the IR spectrum on Pt-$TiO_2$/α-$Al_2O_3$ (Fig. 6b) and Pt/α-$Al_2O_3$ (Fig. S8c) showed decreased absorbance after passing 10% $H_2$/Ar, which is attributed to LA hydrogenation. Compared to Pt/α-$Al_2O_3$, the decay of LA absorption bands for Pt-$TiO_2$/α-$Al_2O_3$ is more pronounced, indicating a higher hydrogenation efficiency. For Pt/α-$Al_2O_3$, only LA was consumed after $H_2$ introduction. In addition to the consumption of LA, α-angelica lactone and Ti-OH species also were consumed over Pt-$TiO_2$/α-$Al_2O_3$ in 10% $H_2$/Ar. Thus, α-angelica lactone was the primary intermediate for LA aqueous-phase hydrogenation due to Pt-$TiO_2$ interaction. And the Ti-OH species is dynamically consumed and generated during the reaction.

## 4. Discussion

Here, we successfully design a Pt-$TiO_2$/α-$Al_2O_3$ with the identical Pt particle size, lattice plane, support morphology, pore structure, and electronic structure as Pt/α-$Al_2O_3$. The special effect of Pt-$TiO_2$ interaction is clearly revealed for LA aqueous-phase hydrogenation. From the results of isotopic experiments, it can be found that there is no isotope effect of $D_2$, indicating that the activation of hydrogen is not the rate-limiting step for the aqueous-phase hydrogenation of LA. Further CO-DRIFT, LA adsorption, and kinetic experiments indicate that the LA adsorption and activation are the critical step and are enhanced due to the Pt-$TiO_2$ interaction.

CO-DRIFT was utilized to reveal the role of the different surface Pt active sites. α sites belonging to Pt-$TiO_2$ peripheral sites can strongly adsorb LA, leading to the enrichment of LA on the surface. And α and β sites were occupied by stable intermediates. In contrast, the γ sites cannot adsorb LA and its intermediates during the hydrogenation. Kinetic experiments and in-situ FTIR results indicate that water participates in the key step for LA hydrogenation on Pt-$TiO_2$/α-$Al_2O_3$ and stimulates the formation of more Ti−OH sites at the Pt-$TiO_2$ interface for LA direct cyclization to α-angelica lactone intermediate. According to

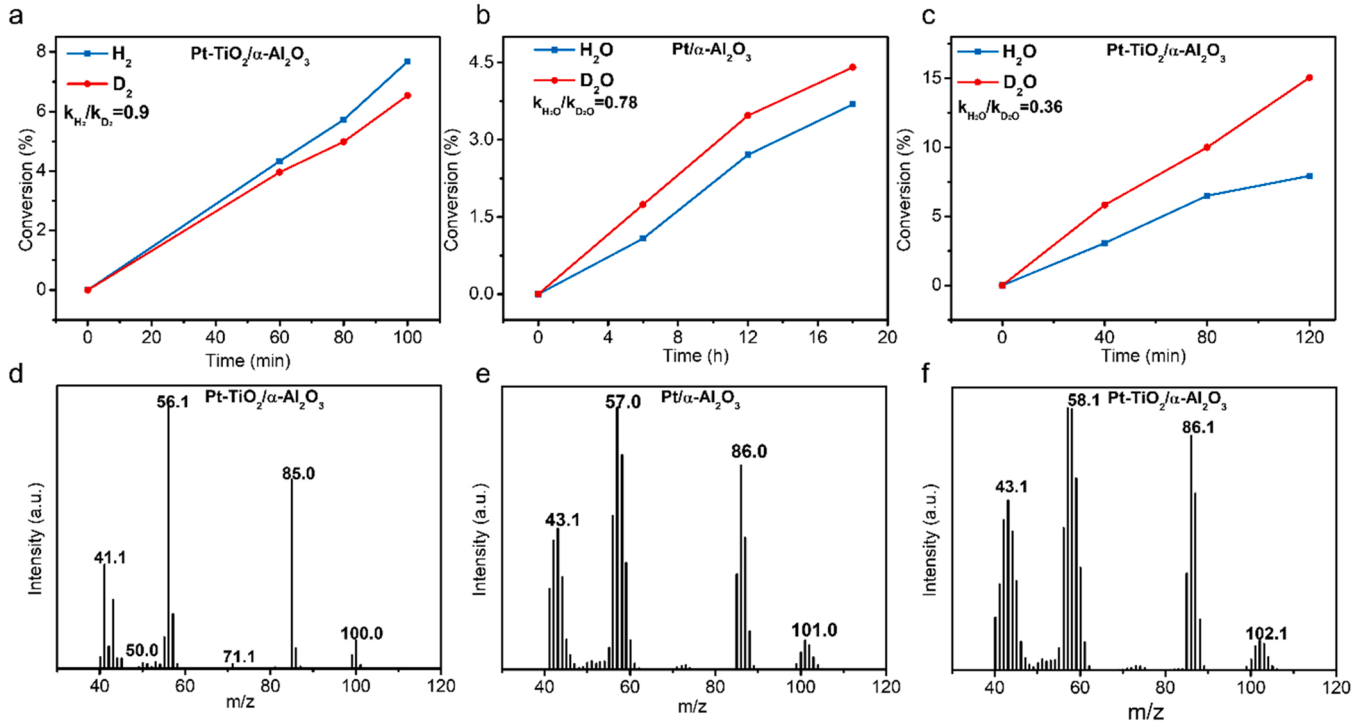


**Fig. 5.** Kinetic isotope effect. (a) $D_2$ isotope effect in the LA hydrogenation over Pt-$TiO_2$/α-$Al_2O_3$. (b) $D_2O$ isotope effect in the LA hydrogenation over Pt/α-$Al_2O_3$. (c) GC-MS spectra of the liquid products catalyzed by Pt /α-$Al_2O_3$ using $D_2O$ instead of $H_2O$. (d) GC-MS spectra of the liquid products catalyzed by Pt-$TiO_2$/α-$Al_2O_3$ using $D_2$ instead of $H_2$. (e) $D_2O$ isotope effect in the LA hydrogenation over Pt-$TiO_2$/α-$Al_2O_3$. (f) GC-MS spectra of the liquid products catalyzed by Pt-$TiO_2$/α-$Al_2O_3$ using $D_2O$ instead of $H_2O$. (Reaction condition: a. 5 mg Pt-$TiO_2$/α-$Al_2O_3$, 2 MPa $H_2$($D_2$),150 °C, 5 mL $H_2O$,700 rpm. b. 5 mg Pt /α-$Al_2O_3$, 3 MPa $H_2$,150 °C, 5 mL $H_2O$ ($D_2O$), 700 rpm. c. 5 mg Pt-$TiO_2$/α-$Al_2O_3$, 3 MPa $H_2$,150 °C, 5 mL $H_2O$ ($D_2O$), 700 rpm).

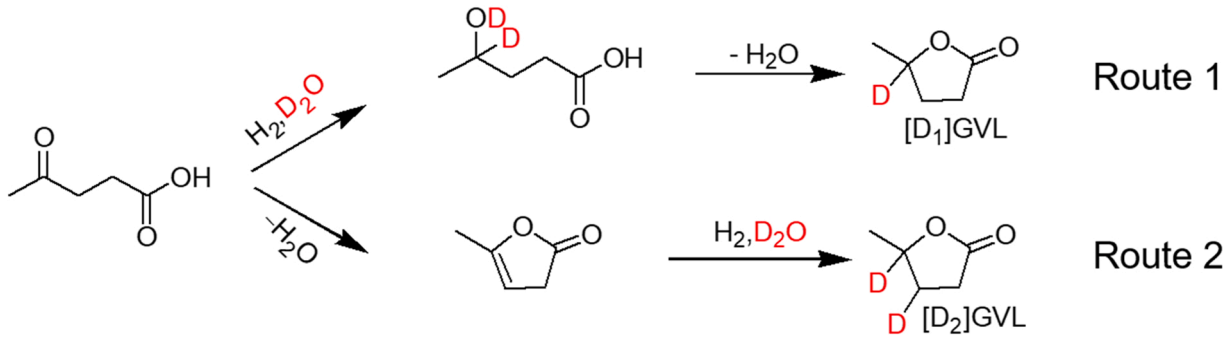


**Scheme 2.** The reaction route of LA hydrogenation to GVL.

these results, we can propose the following reaction mechanism. The surface adsorbed LA at the Pt α sites is first transformed to α-angelica lactone intermediates, which readily undergo further hydrogenation at the Pt α and β sites. Meanwhile, the active hydrogen will be readily formed on Pt γ sites and transformed to Pt α and β sites for hydrogenation. In brief, the high efficiency for aqueous-phase LA hydrogenation origins from the molecular adsorption, dynamic transport, and transformation on multi-sites of Pt-$TiO_2$/α-$Al_2O_3$ in the aqueous phase.

To explore the universality of building Pt-$TiO_2$ interaction for high-efficiency hydrogenation in the aqueous phase, we have deposited the $TiO_2$ layer on different common supports before the deposition of Pt nanoparticles. Moreover, the catalytic properties of these catalysts were examined in LA hydrogenation under the same condition. It can be observed that the catalytic efficiency was all enhanced after the formation of Pt-$TiO_2$ interaction (Fig. 7), indicating the universality of the $TiO_2$ surface overcoating strategy. CO-DRIFTS was used to verify the Pt-$TiO_2$ interaction over different supports. A new species with the decorating of $TiO_2$ originated from the formation of the Pt-$TiO_2$ interaction, which we have observed for Pt-$TiO_2$/α-$Al_2O_3$ (Fig. S9). Moreover, increased Pt loadings are observed after the formation of Pt-$TiO_2$ interaction on different supports (Fig. S10).

## 5. Conclusion

In summary, highly efficient Pt-$TiO_2$/α-$Al_2O_3$ catalyst was synthesized by ALD for aqueous-phase LA hydrogenation. The role of Pt-$TiO_2$ interaction in aqueous-phase LA hydrogenation was investigated after excluding the effects of morphology, pore structure, Pt particle size, lattice plane structure, etc. The Pt-$TiO_2$ interaction provides new active sites for LA adsorption and direct cyclization to an α-angelica lactone intermediate. Compared to Pt/α-$Al_2O_3$, Pt-$TiO_2$/α-$Al_2O_3$ shift the catalytic reaction path with lower activation energy due to the formation of Pt-$TiO_2$ interaction. These findings open up new possibilities for designing high-efficient Pt catalysts for aqueous-phase hydrogenation by precisely designing the metal-oxide interaction.

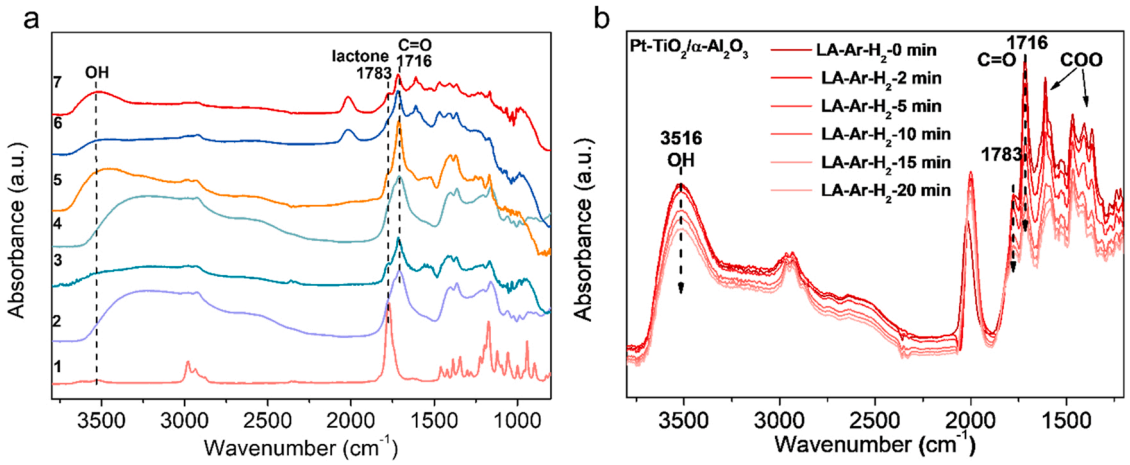


**Fig. 6.** Investigation of Intermediate for aqueous-phase LA hydrogenation. (a) In-situ FTIR difference spectra of the adsorption of LA, GVL, and LA aqueous solution on different samples: (1) GVL on KBr; (2) LA on KBr; (3) the adsorption of LA aqueous solution on $TiO_2/\alpha$-$Al_2O_3$; the adsorption of pure LA on $TiO_2/\alpha$-$Al_2O_3$ (4) and then injection water (5); (6) the adsorption of LA aqueous solution on $Pt/\alpha$-$Al_2O_3$; (7) the adsorption of LA aqueous solution on Pt-$TiO_2/\alpha$-$Al_2O_3$. (b) In-situ FTIR difference spectra of the adsorption LA aqueous solution on Pt-$TiO_2/\alpha$-$Al_2O_3$ as a function of flushing time in 10% $H_2$/Ar flow at 150 °C.

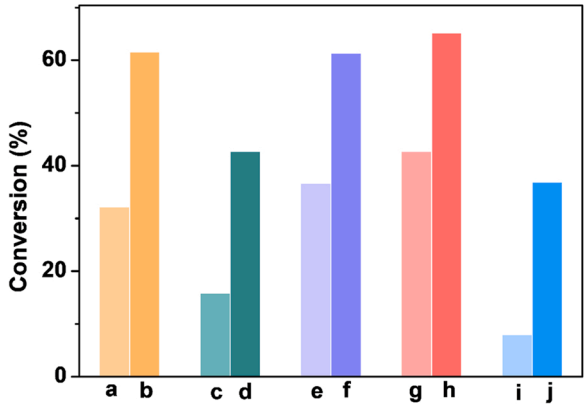


**Fig. 7.** The building Pt-$TiO_2$ interaction on different supports for LA aqueous-phase hydrogenation. $Pt/\gamma$-$Al_2O_3$ (a), Pt-$TiO_2/\gamma$-$Al_2O_3$ (b), $Pt/CeO_2$ (c), Pt-$TiO_2/CeO_2$ (d), $Pt/ZrO_2$ (e), Pt-$TiO_2/ZrO_2$ (f), Pt/P25 (g), Pt-$TiO_2$/P25 (h), $Pt/\alpha$-$Al_2O_3$ (i), Pt-$TiO_2/\alpha$-$Al_2O_3$ (j). (reaction conditions: 10 mg catalyst, 3 MPa, 8.6 mmol LA, 150 °C, 5 mL $H_2O$, 700 rpm, 1 h).

## CRediT authorship contribution statement

Fanchun Meng performed the majority of the synthesis, characterization, and catalytic tests. Xinchun Yang, Zhuo Li, and Yuntao Qi contributed to the LA hydrogenation tests and CO-DRIFT experiments. Shichao Zhao contributed to the synthesis of the catalysts. Guikai Zhang, Guofu Wang, Shengqi Chu and Jing Zhang contributed to the XAFS experiments. Fanchun Meng, Yong Qin and Bin Zhang wrote the paper, with input from all of the other coauthors. Y.Q. and B.Z. directed the research.

## Declaration of Competing Interest

The authors declare that they have no known competing financial interests or personal relationships that could have appeared to influence the work reported in this paper.

## Data availability

No data was used for the research described in the article.

## Acknowledgments

We acknowledge the financial support from the National Natural Science Foundation of China (21872160, 22072172), the National Key R&D Program of China (2018YFB1501602 and 2017YFA0700101), the National Science Fund for Distinguished Young Scholars (21825204), the Youth Innovation Promotion Association CAS (Y2021056), Natural Science Foundation of Shanxi Province (201901D211591), Major Scientific and Technological Special Project of Shanxi Province (202005D121002) and Young Talents Plan of State Key Laboratory of Coal Conversion (2021BWZ005).

## Appendix A. Supporting information

Supplementary data associated with this article can be found in the online version at doi:10.1016/j.apcatb.2022.122236.

## References

[1] P. Hao, D.K. Schwartz, J.W. Medlin, Effect of surface hydrophobicity of $Pd/Al_2O_3$ on vanillin hydrodeoxygenation in a water/oil system, ACS Catal. 8 (2018) 11165–11173, https://doi.org/10.1021/acscatal.8b03141.
[2] G.W. Huber, R.D. Cortright, J.A. Dumesic, Renewable alkanes by aqueous-phase reforming of biomass-derived oxygenates, Angew. Chem. Int. Ed. 116 (2004) 1575–1577, https://doi.org/10.1002/ange.200353050.
[3] M.A. Mellmer, D. Martin Alonso, J.S. Luterbacher, J.M.R. Gallo, J.A. Dumesic, Effects of γ-valerolactone in hydrolysis of lignocellulosic biomass to monosaccharides, Green. Chem. 16 (2014) 4659–4662, https://doi.org/10.1039/c4gc01768d.
[4] B. Mostofian, C.M. Cai, M.D. Smith, L. Petridis, X. Cheng, C.E. Wyman, J.C. Smith, Local phase separation of co-solvents enhances pretreatment of biomass for bioenergyapplications, J. Am. Chem. Soc. 138 (2016) 10869–10878, https://doi.org/10.1021/jacs.6b03285.
[5] T.Y. Nguyen, C.M. Cai, R. Kumar, C.E. Wyman, Co-solvent pretreatment reduces costly enzyme requirements for high sugar and ethanol yields from lignocellulosic biomass, ChemSusChem 8 (2015) 1716–1725, https://doi.org/10.1002/cssc.201403045.
[6] M. Pera-Titus, L. Leclercq, J.M. Clacens, F. De Campo, V. Nardello-Rataj, Pickering interfacial catalysis for biphasic systems: from emulsion design to green reactions, Angew. Chem. Int. Ed. 54 (2015) 2006–2021, https://doi.org/10.1002/anie.201402069.
[7] C. Michel, J. Zaffran, A.M. Ruppert, J. Matras-Michalska, M. Jedrzejczyk, J. Grams, P. Sautet, Role of water in metal catalyst performance for ketone hydrogenation: a joint experimental and theoretical study on levulinic acid conversion into gamma-valerolactone, Chem. Commun. 50 (2014) 12450–12453, https://doi.org/10.1039/c4cc04401k.
[8] J. Tan, J. Cui, T. Deng, X. Cui, G. Ding, Y. Zhu, Y. Li, Water-promoted hydrogenation of levulinic acid to γ-valerolactone on supported ruthenium catalyst, ChemCatChem 7 (2015) 508–512, https://doi.org/10.1002/cctc.201402834.

[9] R. Weng, Z. Yu, J. Xiong, X. Lu, Effects of water in the heterogeneous catalytic valorization of levulinic acid into γ-valerolactone and its derivatives, Green. Chem. 22 (2020) 3013–3027, https://doi.org/10.1039/d0gc01082k.
[10] B. Zhang, Y. Chen, J. Li, E. Pippel, H. Yang, Z. Gao, Y. Qin, High Efficiency Cu-ZnO Hydrogenation Catalyst: The Tailoring of Cu-ZnO Interface Sites by Molecular Layer Deposition, ACS Catal. 5 (2015) 5567–5573, https://doi.org/10.1021/acscatal.5b01266.
[11] O. Mamun, M. Saleheen, J.Q. Bond, A. Heyden, Investigation of solvent effects in the hydrodeoxygenation of levulinic acid to γ-valerolactone over Ru catalysts, J. Catal. 379 (2019) 164–179, https://doi.org/10.1016/j.jcat.2019.09.026.
[12] B. Demir, T. Kropp, E.B. Gilcher, M. Mavrikakis, J.A. Dumesic, Effects of water on the kinetics of acetone hydrogenation over Pt and Ru catalysts, J. Catal. 403 (2021) 215–227, https://doi.org/10.1016/j.jcat.2021.03.013.
[13] X.-m Gu, B. Zhang, H.-j Liang, H.-b Ge, H.-m Yang, Y. Qin, Pt/HZSM-5 catalyst synthesized by atomic layer deposition for aqueous-phase hydrogenation of levulinic acid to valeric acid, J. Fuel Chem. Tech. 45 (2017) 714–722, https://doi.org/10.1016/s1872-5813(17)30035-x.
[14] M. Ahmadi, H. Mistry, B. Roldan Cuenya, Tailoring the catalytic properties of metal nanoparticles via support interactions, J. Phys. Chem. Lett. 7 (2016) 3519–3533, https://doi.org/10.1021/acs.jpclett.6b01198.
[15] J. Chang, Y. Zhang, Y. Yao, X. Liu, D. Hildebrandt, Reduced graphene oxide supported cobalt catalysts for ethylene hydroformylation: Modified cobalt-support interaction by rhodium, Fuel 324 (2022) 124479–124486, https://doi.org/10.1016/j.fuel.2022.124479.
[16] T.W. van Deelen, C. Hernández Mejía, K.P. de Jong, Control of metal-support interactions in heterogeneous catalysts to enhance activity and selectivity, Nat. Catal. 2 (2019) 955–970, https://doi.org/10.1038/s41929-019-0364-x.
[17] P. Sudarsanam, H. Li, T.V. Sagar, TiO2-based water-tolerant acid catalysis for biomass-based fuels and chemicals, ACS Catal. 10 (2020) 9555–9584, https://doi.org/10.1021/acscatal.0c01680.
[18] X.Y. Shi, W. Zhang, C. Zhang, W.T. Zheng, H. Chen, J.G. Qi, Real-space observation of strong metal-support interaction: state-of-the-art and what's the next, J. Microsc. 262 (2016) 203–215, https://doi.org/10.1111/jmi.12366.
[19] A.V.-H. Soares, G. Perez, F.B. Passos, Alumina supported bimetallic Pt–Fe catalysts applied to glycerol hydrogenolysis and aqueous phase reforming, Appl. Catal. B: Environ. 185 (2016) 77–87, https://doi.org/10.1016/j.apcatb.2015.11.003.
[20] A. Fernández, G.M. Arzac, U.F. Vogt, F. Hosoglu, A. Borgschulte, M.C. Jiménez de Haro, O. Montes, A. Züttel, Investigation of a Pt containing washcoat on SiC foam for hydrogen combustion applications, Appl. Catal. B: Environ. 180 (2016) 336–343, https://doi.org/10.1016/j.apcatb.2015.06.040.
[21] H. Liang, B. Zhang, H. Ge, X. Gu, S. Zhang, Y. Qin, Porous $TiO_2$/Pt/$TiO_2$ Sandwich Catalyst for Highly Selective Semihydrogenation of Alkyne to Olefin, ACS Catal. 7 (2017) 6567–6572, https://doi.org/10.1021/acscatal.7b02032.
[22] Y. Zhou, D.E. Doronkin, M. Chen, S. Wei, J.-D. Grunwaldt, Interplay of Pt and Crystal Facets of $TiO_2$: CO Oxidation Activity and Operando XAS/DRIFTS Studies, ACS Catal. 6 (2016) 7799–7809, https://doi.org/10.1021/acscatal.6b01509.
[23] W. Luo, M. Sankar, A.M. Beale, Q. He, C.J. Kiely, P.C. Bruijnincx, B. M. Weckhuysen, High performing and stable supported nano-alloys for the catalytic hydrogenation of levulinic acid to gamma-valerolactone, Nat. Commun. 6 (2015) 6540, https://doi.org/10.1038/ncomms7540.
[24] M. Primet, Electronic transfer and ligand effects in the infrared-spectra of adsorbed carbon-monoxide, J. Catal. 88 (1984) 273–282, https://doi.org/Doi 10.1016/0021-9517(84)90003-4.
[25] P.T. Fanson, W.N. Delgass, J. Lauterbach, Island Formation during Kinetic Rate Oscillations in the Oxidation of CO over Pt/$SiO_2$: A Transient Fourier Transform Infrared Spectrometry Study, J. Catal. 204 (2001) 35–52, https://doi.org/10.1006/jcat.2001.3369.
[26] P. Hollins, The influence of surface-defects on the infrared-spectra of adsorbed species, Surf. Sci. Rep. 16 (1992) 51–94, https://doi.org/Doi10.1016/0167-5729(92)90008-Y.
[27] M. Macino, A.J. Barnes, S.M. Althahban, R. Qu, E.K. Gibson, D.J. Morgan, S. J. Freakley, N. Dimitratos, C.J. Kiely, X. Gao, A.M. Beale, D. Bethell, Q. He, M. Sankar, G.J. Hutchings, Tuning of catalytic sites in Pt/$TiO_2$ catalysts for the chemoselective hydrogenation of 3-nitrostyrene, Nat. Catal. 2 (2019) 873–881, https://doi.org/10.1038/s41929-019-0334-3.
[28] T. Avanesian, S. Dai, M.J. Kale, G.W. Graham, X. Pan, P. Christopher, Quantitative and Atomic-Scale View of CO-Induced Pt Nanoparticle Surface Reconstruction at Saturation Coverage via DFT Calculations Coupled with in Situ TEM and IR, J. Am. Chem. Soc. 139 (2017) 4551–4558, https://doi.org/10.1021/jacs.7b01081.
[29] M.J. Kale, P. Christopher, Utilizing Quantitative in Situ FTIR Spectroscopy To Identify Well-Coordinated Pt Atoms as the Active Site for CO Oxidation on $Al_2O_3$-Supported Pt Catalysts, ACS Catal. 6 (2016) 5599–5609, https://doi.org/10.1021/acscatal.6b01128.
[30] H.V. Thang, G. Pacchioni, L. DeRita, P. Christopher, Nature of stable single atom Pt catalysts dispersed on anatase $TiO_2$, J. Catal. 367 (2018) 104–114, https://doi.org/10.1016/j.jcat.2018.08.025.
[31] C.R. Werrett, A.K. Bhattacharya, D.R. Pyke, The validity of Cls charge referencing in the XPS of oxidized Al-Si alloys, Appl. Sur. Sci. 103 (1996) 403–407, https://doi.org/10.1016/s0169-4332(96)00539-9.
[32] E.L. Kunkes, F. Studt, F. Abild-Pedersen, R. Schlögl, M. Behrens, Hydrogenation of $CO_2$ to methanol and CO on Cu/ZnO/$Al_2O_3$: Is there a common intermediate or not? J. Catal. 328 (2015) 43–48, https://doi.org/10.1016/j.jcat.2014.12.016.
[33] K.S. Rangappa, K. Manjunathaswamy, M.P. Raghavendra, N.M. Made Gowda, Kinetics and mechanism of oxidation of neutral α-amino acids by sodium N-chloro-p-toluenesulfonamide in acid medium, Int. J. Chem. Kinet. 34 (2002) 49–55, https://doi.org/10.1002/kin.10011.
[34] J. Du, Z. Chen, C. Chen, T.J. Meyer, A half-reaction alternative to water oxidation: chloride oxidation to chlorine catalyzed by silver ion, J. Am. Chem. Soc. 137 (2015) 3193–3196, https://doi.org/10.1021/jacs.5b00037.
[35] D. Gong, V.P. Subramaniam, J.G. Highfield, Y. Tang, Y. Lai, Z. Chen, In Situ Mechanistic Investigation at the Liquid/Solid Interface by Attenuated Total Reflectance FTIR: Ethanol Photo-Oxidation over Pristine and Platinized $TiO_2$ (P25), ACS Catal. 1 (2011) 864–871, https://doi.org/10.1021/cs200063q.
[36] R.A. Farrar-Tobar, A. Dell'Acqua, S. Tin, J.G. de Vries, Metal-catalysed selective transfer hydrogenation of α,β-unsaturated carbonyl compounds to allylic alcohols, Green. Chem. (2020) 3323–3357, https://doi.org/10.1039/D0GC00855A.
[37] J.D. Ferguson, A.R. Yoder, A.W. Weimer, S.M. George, $TiO_2$ atomic layer deposition on $ZrO_2$ particles using alternating exposures of $TiCl_4$ and $H_2O$, Appl. Sur. Sci. 226 (2004) 393–404, https://doi.org/10.1016/j.apsusc.2003.10.053.
[38] V.K. Velisoju, G.B. Peddakasu, N. Gutta, V. Boosa, M. Kandula, K.V.R. Chary, V. Akula, Influence of Support for Ru and Water Role on Product Selectivity in the Vapor-Phase Hydrogenation of Levulinic Acid to γ-Valerolactone: Investigation by Probe-Adsorbed Fourier Transform Infrared Spectroscopy, J. Phy. Chem. C. 122 (2018) 19670–19677, https://doi.org/10.1021/acs.jpcc.8b06003.
[39] H. Wu, B. Zhang, H. Liang, L. Zhai, G. Wang, Y. Qin, Distance effect of Ni-Pt dual sites for active hydrogen transfer in tandem reaction, The Innovation 1 (2020), 100029, https://doi.org/10.1016/j.xinn.2020.100029.